

Variable and Polarised Near-infrared Emission from the Galactic Centre

Banafsheh Shahzamanian^{1,2}
 Andreas Eckart^{1,2}
 Monica Valencia-S.¹
 Gunther Witzel³
 Mohammad Zamaninasab²
 Michal Zajaček^{1,2,4}
 Nadeen Sabha¹
 Macarena García-Marín¹
 Vladimir Karas⁴
 Florian Peissker¹
 Grischa D. Karssen¹
 Marzieh Parsa¹
 Nicolas Grosso⁵
 Enmanuelle Mossoux⁵
 Delphine Porquet⁵
 Behrang Jalali¹
 Matthew Horrobin¹
 Rainer Buchholz¹
 Michal Dovčiak⁴
 Devaky Kunneriath⁴
 Michal Bursa⁴
 Anton Zensus^{2,1}
 Rainer Schödel⁶
 Jihane Moultaq⁷
 Christian Straubmeier¹

¹ I. Physikalisches Institut der Universität zu Köln, Germany

² Max-Planck-Institut für Radioastronomie, Bonn, Germany

³ Department of Physics and Astronomy, University of California, Los Angeles, USA

⁴ Astronomical Institute of the Academy of Sciences, Prague, Czech Republic

⁵ Observatoire Astronomique de Strasbourg, Université de Strasbourg, CNRS, UMR 7550, Strasbourg, France

⁶ Instituto de Astrofísica de Andalucía (CSIC), Granada, Spain

⁷ Université de Toulouse III – CNRS – IRAP, Observatoire Midi-Pyrénées, France

Infrared observations of the Galactic Centre (GC) provide a unique opportunity to study stellar and bow-shock polarisation effects in a dusty environment. For the infrared counterpart of the supermassive black hole Sgr A* these observations reveal new insights into the physical processes at work. The observations were carried out with NACO in the Ks-band (2.2 μm) from 2004 to 2012 and several linearly polarised flares were observed during these years. We find that the distribution of

polarised flux density is closely related to the single-state power-law distribution of the total flux densities. A typical polarisation degree of the order of 10–20 % and a preferred polarisation angle of $13^\circ \pm 15^\circ$ are derived, likely linked to the intrinsic orientation of the Sgr A* system. We discuss different scenarios for the accretion process for the Sgr A* system based on our findings.

Introduction

Sagittarius A* (Sgr A*) is a compact radio source associated with the supermassive black hole of four million solar masses located at the centre of the Galaxy. It is the galactic nucleus nearest to us. Sgr A* is time variable in the near-infrared (NIR) and X-ray regimes, and also in the radio to submillimetre domain but with a lower degree of variability.

Studying the polarisation of the electromagnetic radiation helps us to understand the underlying physics governing the emission mechanism of Sgr A*. The polarised NIR flux density excursions often exhibit X-ray counterparts, which suggests synchrotron-self-Compton (SSC) or inverse Compton emission as the mechanisms responsible for the radiation (Eckart et al., 2012). Several relativistic models that match the observations assume the variability of Sgr A* to be related to the accretion process and, in particular, to emission from matter close to the last stable orbit around the

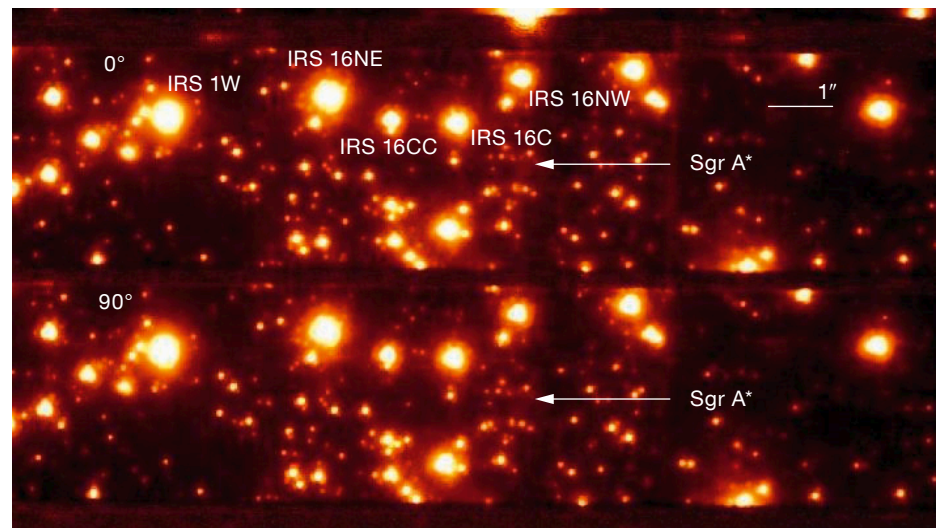
black hole. Correlations between the modulations of the observed flux density light curves and changes in polarisation degree and angle are expected from models where matter is orbiting the supermassive black hole Sgr A* at relativistic speed (e.g., Zamaninasab et al., 2010).

The time-variable NIR emission from Sgr A* can be understood as a result of a single continuous power-law process (Witzel et al., 2012). This continuous process shows a break timescale around a few hundred minutes at which the Fourier power in the flux variability drops. Extreme flux density excursions typically last for about 100 minutes and these excursions are referred to as flares. Here we report on the most comprehensive sample of NIR polarimetric data for Sgr A*.

Polarimetry with NACO

All observations have been carried out with the adaptive optics (AO) module NAOS and NIR camera CONICA (together NACO) at Unit Telescope 4 (Yepun) at the Very Large Telescope (VLT). We collected all Ks-band (2.2 μm) data of the central cluster at the Galactic Centre in 13 milli-arcsecond (mas) pixel-scale polarimetric

Figure 1. The arrangement of the Wollaston prism images on the NACO detector. The two central strips show the images in orthogonally polarised light. Another exposure with the retarder rotated by 45° provides a complementary pair of orthogonal measurements from which the full linear polarisation information can be derived.



imaging from mid-2004 to mid-2012 that exhibits flaring activities. The infrared wavefront sensor of NAOS was used for locking the AO loop on the NIR super-giant IRS7 with $K_s \sim 6.5\text{--}7.0$ mag, located ~ 5.5 arcseconds north of Sgr A*. NACO is equipped with a Wollaston prism combined with a half-wave retarder plate that allows simultaneous measurements of two orthogonal directions of the electric field vector and a rapid change between different angles of the electric field vector. A typical pointing towards the Galactic Centre is shown in Figure 1.

The non-normalised analogue-to-digital converter (ADC) values from the detector were directly used to obtain the normalised Stokes parameters, Q and U , and to derive the linear polarisation degree p and angle ϕ (see Equations 1–5 in Shahzamanian et al., 2014). The polarised flux density was computed as a product of the degree of polarisation and the total flux density. Uncertainties for Q , U and the obtained p and ϕ were determined from the flux density uncertainties. The model derived by Witzel et al. (2011) was employed to reduce the systematic uncertainties of polarisation angles and degrees caused by instrumental polarisation to about $\sim 1\%$ and $\sim 5^\circ$ respectively.

Polarised flux in the central stellar cluster

Using AO-assisted K_s - ($2.2\ \mu\text{m}$) and L' -band ($3.8\ \mu\text{m}$) observations with NACO (Buchholz et al., 2011; 2013), high-precision photometry and the new polarimetric calibration method, the polarisation of the Galactic Centre stellar cluster including Sgr A* was mapped (Witzel et al., 2011; Shahzamanian et al., 2014). In the L' -band these are the first polarimetric observations of the GC for 30 years. The vastly improved spatial resolution allows resolved polarimetry on bright bow-shock sources in this area for the first time at this wavelength. The foreground polarisation is largely parallel to the Galactic Plane (K_s -band: 6.1% at 20° ; L' -band: 4.5% at 20°). The bow-shock sources like IRS 1W and 21 clearly show contributions from intrinsic K_s - and L' -band polarisation. The data provided support for the presumed bow-shock nature of several of these sources (IRS 1W, 5, 5NE, 10W and 21) and for the model of bow-shock polarisa-

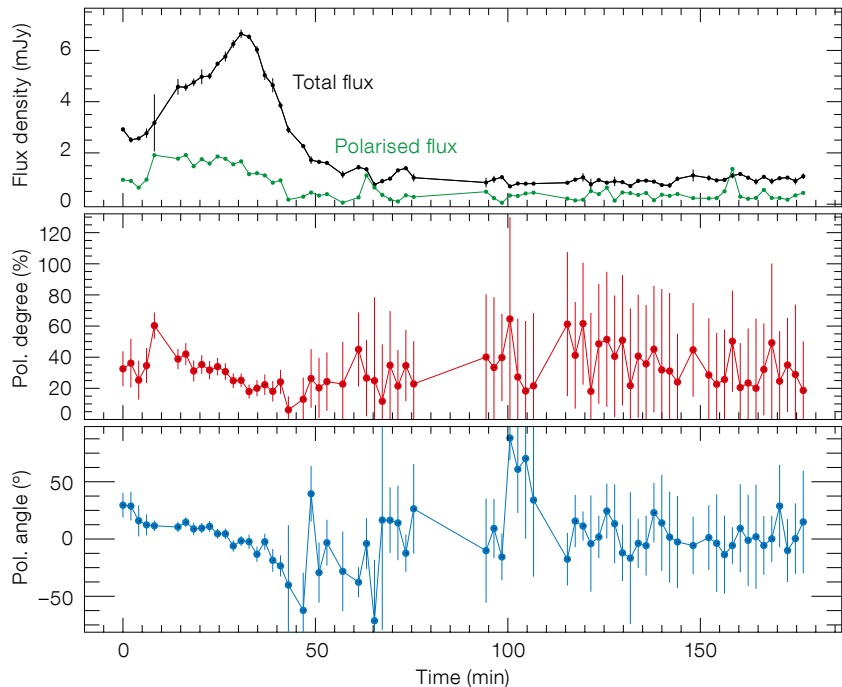


Figure 2. Flare observed in NIR K_s -band polarimetry mode of Sgr A* on 17 May 2012. Top: Total flux density (black) and polarised flux density (green) measured in mJy; Middle: Linear polarisation degree (orange); Bottom: Linear polarisation angle (blue).

tion. For the stellar sources, the origin of the polarised emission arises from a combination of scattering and selective dichroic absorption and emission of dust. In the case of Sgr A*, strongly time-variable polarisation is a clear indication for intrinsic emission mechanisms (such as synchrotron emission) at work, which provide strongly polarised radiation. Figure 2 shows a light curve resulting from typical Sgr A* measurements with NACO in polarisation mode. For high flare flux, the polarisation degree and angle are very well defined.

Sgr A*: Analysis of polarisation degree and angle

We analysed polarised NIR light curves of Sgr A* covering the years 2004 to 2012. A detailed description is given by Shahzamanian et al. (2014). In order to interpret the data it is important to take into account the statistical behaviour of the polarisation measurements. Polarisation degree p is a positive quantity that takes values between zero and one (or, equivalently, 0–100%). The uncertainties

in Q and U , which in our case are the result of observational noise in the polarisation channels, bias the value of p . This leads to an overestimate of p at low signal-to-noise (S/N) measurements. Moreover, polarimetric observations require a higher S/N compared to photometric measurements. Monte Carlo simulations of the measured intensities and their uncertainties in the polarisation channels were performed to derive the expected uncertainties in p and ϕ for different S/N ratios.

Simulations show that for intrinsic flux lower than ~ 2 mJy the recovered polarisation degree is not Gaussian distributed, and especially for low intrinsic polarisation degrees the intrinsic value is not recovered with satisfactory confidence and the uncertainties are very large. On the other hand, for weak flares that are intrinsically strongly polarised, the intrinsic polarisation degrees are statistically recovered, but the asymmetric uncertainties remain large. Therefore, the total statistical behaviour of the observed polarisation data is composed of the properties of subsamples of different polarisation degrees and flare flux.

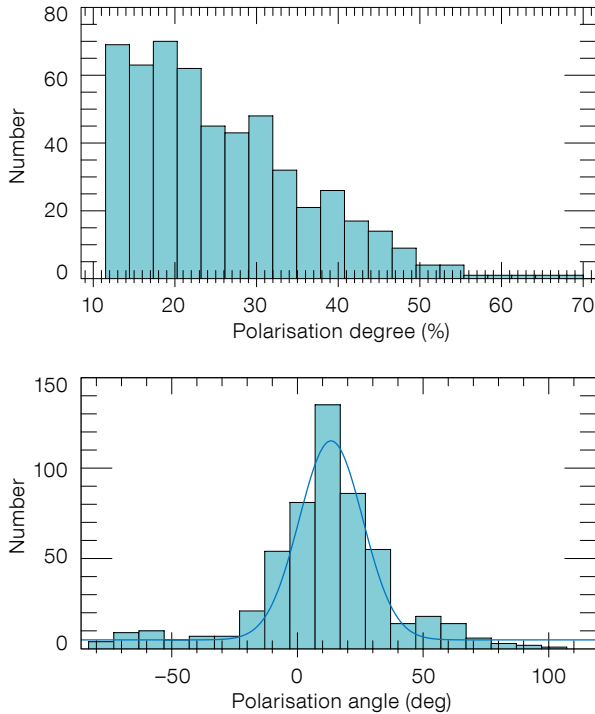


Figure 3. Histogram of the result from all light curves of Sgr A* observed in polarised Ks-band obtained in 2004–2012. Upper: Distribution of polarisation degree; Lower: Distribution of polarisation angle. The dark blue line shows the fit with a Gaussian distribution.

In Figure 3 (upper plot) the distribution of the Ks-band polarisation degree of Sgr A* is shown. Only the significant measurements are plotted, i.e., successful retrievals of the intrinsic p and ϕ . The distribution of p does not have a Gaussian shape: it is flat until $\sim 20\%$ and then starts dropping towards smaller values and is also strongly influenced by systematic effects with uncertainties of several tens of percent. Figure 3 (lower) shows the distribution of significant Ks-band polarisation angles for Sgr A*. The distribution of ϕ shows a peak at 13° and has a width of the order of 30° , therefore, the preferred polarisation angle that can be derived from the distribution is $13^\circ \pm 15^\circ$ (see Figure 4). The distribution of ϕ can be described by a Gaussian function that peaks at the preferred value whose width then corresponds to the combined effect of the intrinsic polarisation angle variability and the measurement uncertainties.

In general, the linear polarisation is linked in degree and angle to the magnetic field structure and the source geometry.

In the case of Sgr A*, neither is it clear whether it has a permanent accretion disc nor whether it has a permanent jet. All of these structures may occur as transient phenomena and then affect the properties of the expected polarisation degree and angle due to the corresponding emission mechanisms. It is very likely that the NIR flare emission originates from optically thin synchrotron radiation (Eckart et al., 2012). Hence one may expect a link between the preferred NIR polarisation angle and the NIR/radio structure of Sgr A*. At millimetre wavelengths the interstellar scattering is small and allows insight into the intrinsic source structure of Sgr A*. Bower et al. (2014) find an intrinsic major axis position angle of the structure of $95^\circ \pm 10^\circ$ (3σ). This angle of the radio structure is, within the uncertainties, orthogonal to the preferred infrared polarisation angle (see Figure 4).

In a range of position angles between 120° and 130° one finds a few elongated NIR features and an elongated X-ray feature (see Figure 4, and Figure 9 in Eckart et al. [2006]). These features may

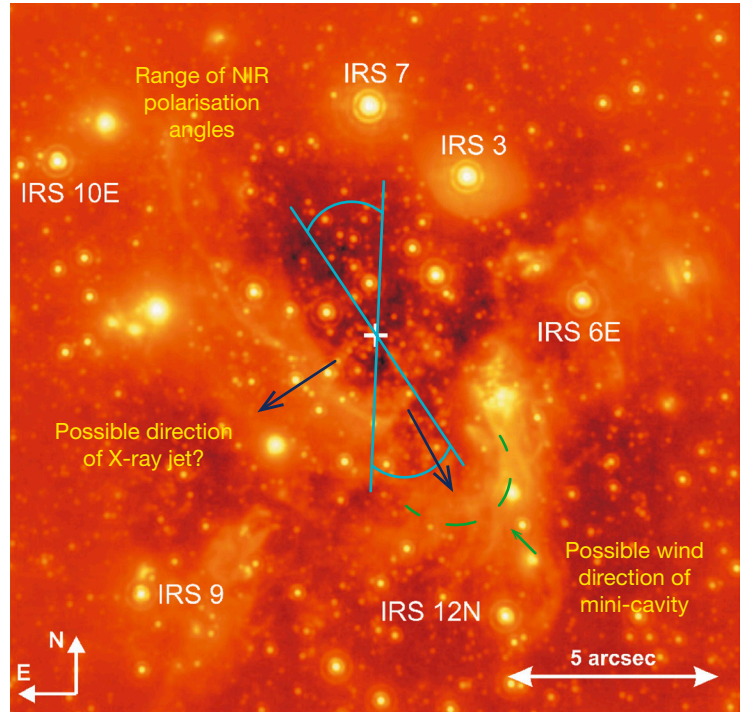


Figure 4. Direction of intrinsic polarisation angle of Sgr A* in the Galactic Centre. The cyan lines include the range over which the NIR polarisation angle varies. The dark blue arrows summarise results from imaging and spectroscopy observation from the radio to X-ray domain: a) the direction of a possible wind responsible for the formation of the mini-cavity; and b) a jet almost perpendicular to it. The green dashed line indicates the wind front of the mini-cavity. Several of the key infrared sources in the region are also indicated.

be associated with a jet phenomenon. In this case the preferred NIR polarisation angle may be associated with the jet components close to or at the foot point of the jet; the polarisation of these components may be along or perpendicular to the jet direction.

It is also possible that the NIR emission originates in hot spots on an accretion disc in a sunspot-like geometry, in which the electric vector is mainly perpendicular to the equatorial plane. The mini-cavity (wind front shown as a dashed line in Figure 4), which may be caused by a collimated outflow from Sgr A*, is located at a position angle of about 193° (i.e. $13^\circ + 180^\circ$; see also Li et al. [2013]). The cometary tails of sources X3 and X7 (Muzic et al., 2010) present additional observational support for the fast wind from Sgr A* at that

position angle. It is unclear how the wind may be related to the possible jet: either there is an additional outflow to the jet, the X-ray feature is not related to the jet, or the mini-cavity was created when the outflow geometry was different.

The distribution of polarisation angles of Sgr A* is not dependent on the strength of the flare and the position of this source in the sky or the instrumental orientation. Instead, the preferred polarisation angle of 13° is a source-intrinsic property. For strong flares, disturbing measuring effects are small and the polarisation degree during these flares is much stronger than that of the background. From these flares we have a direct insight into the source-intrinsic polarised variable infrared emission.

The polarised flux density distribution

The histogram of the polarised flux density distribution of Sgr A* for the fraction of data which is significant is shown in Figure 5. In this histogram the distribution is normalised by the total number of points and the bin size. The distribution of measured polarised flux densities is found to be much broader in comparison to the corresponding distribution of total flux density measurements as presented by Witzel et al. (2012), which were found to be consistent with a single-state emission process. The broader distribution can be explained by the convolution of an intrinsic relative frequency total flux density histogram applied to a range of individual polarisation states; see Shahzamanian et al. (2014) for more details.

Our simulations have shown that the polarisation degree can be recovered with a small uncertainty only for the bright flare flux. Therefore, the properties of the polarised flux density distribution — i.e., the product of the polarisation degree and the total flux density (Figure 5) — can be investigated best for high levels of polarised flare flux. A power-law fit to the data at high flux densities is shown as a dot-dashed red line. For high flare flux, the fit results in a slope, $\alpha = 4.00 \pm 0.15$, which is very close to the value of 4.21 ± 0.05 obtained for the total flux density distribution by Witzel et al. (2012).

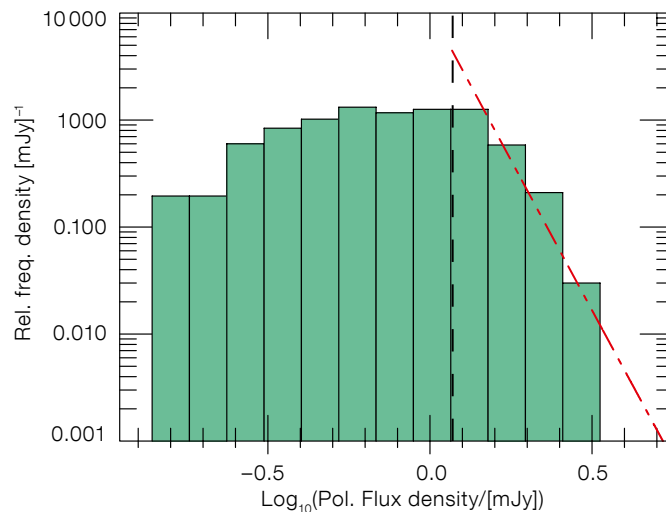


Figure 5. Histogram of polarised flux density (total flux density times polarisation degree) for all significant data is shown with a logarithmic scale, after correction for stellar contamination. The slope at the high flux end compares very well with the slope found for the total flux density.

Recovering this exponent for the polarised flare flux density distribution indicates that the intrinsic polarisation degree is centred around a fixed expectation value and has not varied strongly over the time interval from 2004 to 2012.

The dusty S-cluster object

Gillessen et al. (2012) reported a fast-moving infrared excess source which they interpret as a core-less gas and dust cloud (G2) approaching Sgr A* on an elliptical orbit. Eckart et al. (2014a) present Ks-band identifications and proper motions of the dusty S-cluster object (DSO) derived from VLT and Keck continuum imaging data. In Valencia-S. et al. (2015) new near-infrared (1.45–2.45 μm) observations of the DSO during its approach to the black hole at the centre of the Galaxy are reported; they were carried out with SINFONI at the VLT from February to September 2014. With SINFONI, spatially compact Brackett- γ line emission was detected from DSO/G2 at all epochs before and after its peribothron passage and are in agreement with the detection reported by Witzel et al. (2014) from L-band observations in March 2014.

Combining these observational facts indicates that the DSO is possibly associated with a young accreting stellar object (e.g., a young star; see references given in Valencia-S. et al., 2015) on an elliptical orbit around Sgr A* formed through a process outlined by Jalali et al.

(2014). The observational data were also used to derive the orbit of this object and to predict its periastron transition. With the ellipticity $e = 0.976$ and the half-axis length of 33 mpc, a peribothron distance of about 163 ± 16 au is obtained, which is comparable to previous estimates (e.g., Meyer et al., 2014) and indicates that even if the DSO is an embedded star, its outer shell may very well be subject to tidal disruption (Eckart et al., 2013; Witzel et al., 2014; Zajaček et al. 2014).

Our polarisation statistics show that Sgr A* must be a very stable system, both in terms of geometrical orientation of a jet/wind or an accretion disc and in terms of the variability spectrum that must be linked to the accretion process. The close fly-by of the DSO or similar dusty sources (e.g., Eckart et al., 2014a) might have an effect on the accretion flow onto Sgr A* that depends on the nature of these objects (Zajaček et al., 2014; Jalali et al., 2014). Hence, polarisation and variability measurements of Sgr A* need to be continued as they are the ideal tool to probe any change in the apparently very stable system as a function of the DSO fly-by.

Summary and prospects

We have analysed the near-infrared light curves obtained with NACO at the VLT for Sgr A* at the centre of the Milky Way. Both the steep spectral index (Bremer et al. [2011] and references therein) and the strong variability in the NIR demon-

strate that we are most likely dealing with optically thin synchrotron radiation. Therefore, all properties based on the observation of variable polarised NIR radiation can be directly interpreted as source-intrinsic properties. Some of the main results are depicted in Figure 4 and can be summarised in the following points:

- For flare flux above 5 mJy a range of polarisation degrees of 10–30% is found. If the variable polarised flux from Sgr A* is due to optically thin synchrotron radiation this may indicate depolarisation due to a spatially unresolved complex source structure. For low flare flux the polarisation degree and angle are dominated by measuring uncertainties.
- There is a preferred variable polarisation angle of $13^\circ \pm 15^\circ$. Corrected or the measuring uncertainties, the intrinsic variability of Sgr A* is of the order of 10%. The angle may be linked to jet/wind directions of the corresponding orientation of a temporary accretion disc.
- For the number density distribution of the polarised flux densities, a power-law slope of ~ 4 is found, which is very close to the slope in number density distribution of the total flux densities.
- The well-defined preferred ranges in polarisation degree and angle as

well as the number density power-law slope of four suggest that over the past eight years the geometry and accretion process for the Sgr A* system have been rather stable.

Further progress in investigating the faint polarisation states of Sgr A* in the NIR will require a higher angular resolution in order to better discriminate Sgr A* against background contamination. It is also of interest to use the well-defined NIR polarisation properties of Sgr A* to better determine the apparent stability of the geometrical structure of the system and potentially use variations in this stability to trace interactions of the super-massive black hole at the centre of the Milky Way with its immediate environment.

The known properties of the NACO camera as well as the known polarisation properties of Sgr A* and (most importantly) the many stars in the central cluster that serve as secondary calibrators will allow us to perform a sensitive test of the polarisation characteristics of the new UT1/NACO combination after the move from UT4-Yepun.

Acknowledgements

We acknowledge support through the International Max Planck Research School (IMPRS) for Astronomy

and Astrophysics and the Bonn–Cologne Graduate School (BCGS) for Physics and Astronomy and the University of Cologne. We received funding and support through the FP7/2007-2013 agreement No.312789, the DFG grant SFB 956, the DAAD/Czech MSMT grant (Effects of Albert Einstein’s General Relativity Revealed), and the EU COST Actions MP0905 and MP1104.

References

- Bower, G. C. et al. 2014, *ApJ*, 790, 1
 Bremer, M. et al. 2011, *A&A*, 532, A26
 Buchholz, R. M. et al. 2013, *A&A*, 557, A82
 Buchholz, R. M. et al. 2011, *A&A*, 534, A117
 Eckart, A. et al. 2012, *Journal of Physics Conference Series*, 372, 012022
 Eckart, A. et al. 2014a, in *IAU Symposium*, Vol. 303, ed. Sjouwerman, L. O., Lang, C. C. & Ott, J., 269
 Eckart, A. et al. 2013, *A&A*, 551, A18
 Eckart, A. et al. 2006, *A&A*, 455, 1
 Eckart, A. et al. 2014b, *The Astronomer’s Telegram*, 6285, 1
 Gillessen, S. et al. 2012, *Nature*, 481, 51
 Jalali, B. et al. 2014, *MNRAS*, 444, 1205
 Li, Z., Morris, M. R. & Baganoff, F. K. 2013, *ApJ*, 779, 154
 Meyer, L. et al. 2014, in *IAU Symposium*, Vol. 303, ed. Sjouwerman, L. O., Lang, C. C. & Ott, J., 264
 Muzic, K. et al. 2010, *A&A*, 521, A13
 Shahzamanian, B. et al. 2014, *A&A*, in press, arXiv:1411.0006
 Valencia-S., M. et al. 2015, *ApJ*, 800, 125
 Witzel, G. et al. 2012, *ApJS*, 203, 18
 Witzel, G. et al. 2011, *A&A*, 525, A130
 Witzel, G. et al. 2014, *ApJ*, 796, L8
 Zajaček, M., Karas, V. & Eckart, A. 2014, *A&A*, 565, A17
 Zamaninasab, M. et al. 2010, *A&A*, 510, A3



Observing the Galactic Centre with the VLT’s Unit Telescope 4 with the aid of a laser guide star. See potw1045 for more information.

Y. Beletsky/ESO